

Observations of the shelf break current in the southern Weddell Sea: seasonal variability and mean state

E. Darelius¹, I. Fer¹, M. Janout², K. Daae¹ and N. Steiger³

¹Geophysical Institute, University of Bergen and the Bjerknes Centre for Climate Research, Bergen, Norway

²Alfred-Wegener-Institute Helmholtz Center for Polar and Marine Research, Bremerhaven, Germany

³Sorbonne Université, CNRS/IRD/MNHN, LOCEAN-IPSL, Paris, France

Key Points:

- Four years of observations show that the Antarctic Slope current north of the Filchner Trough is bottom enhanced and strongest during winter
- On the upper part of the slope, the thermocline slopes upward towards the shelf break, and more so for warmer isotherms
- On monthly time scales, positive temperature anomalies are associated with weaker-than-normal currents and vice versa.

Corresponding author: Elin Darelius, elin.darelius@uib.no

Abstract

The Antarctic Slope Front and the associated Antarctic Slope Current are central in determining the dynamics along and the exchanges across the continental shelf break around Antarctica. Here, we present new, four-year-long (2017-2021) records from two moorings deployed on the upper part of the continental slope (530 m and 738 m depth) just upstream of the Filchner Trough in the southern Weddell Sea. We use the records to describe the mean state and the seasonal variability of the shelf break current and the regional hydrography. We find that (i) the current is bottom enhanced, (ii) the isotherms slope upwards towards the shelfbreak, and more so for warmer isotherms, and (iii) the monthly mean thermocline depth is shallowest in February-March and deepest in May-June while (iv) the current is strongest in April-June. On monthly timescales, we show that (v) positive (warm) temperature anomalies of the de-seasoned records are associated with weaker-than-usual currents. Our results contribute to the understanding of how warm ocean waters propagate southward and potentially affect basal melt rates at the Filchner-Ronne Ice Shelf.

Plain Language Summary

The Antarctic ice shelves are melting at an accelerating rate. A large fraction of the melt occurs within the ice shelf cavities, and the heat needed to melt the ice comes from "warm water" originating in the deep ocean. The "warm" water is transported towards the cavities across the relatively shallow continental shelves by ocean currents. The Antarctic Slope Current, a current that flows along the continental slope, and the associated front (i.e the border between cold and warm water masses) limit the amount of "warm" water that enters the continental shelf. Here, we use new four-year-long mooring records from the upper part of the continental slope just east of the Filchner Trough in the southern Weddell Sea to study this current. We find that the strength of current increases towards the bottom and that it has a strong seasonal cycle with a maximum in April-June and a minimum in austral summer. The warm water shoals towards the shelf break and it is found 200 m shallower in February than in winter. Our results contribute to the understanding of how warm ocean waters propagate southward and potentially affect basal melt rates at the Filchner-Ronne Ice Shelf.

1 Introduction

The Antarctic Slope Front (ASF) is a thermohaline front that separates the cold waters on the shallow continental shelf from the comparatively warm Circumpolar Deep Water (CDW) found at depth off the continental shelf (Whitworth et al., 1998; Orsi et al., 2002). The ASF is formed as prevailing easterly winds and southward surface Ekman transport cause surface water to converge along the coast, elevating the sea surface along the Antarctic coastline and depressing the isopycnals (Ekman pumping, Sverdrup, 1953). The ASF dynamically supports the Antarctic Slope Current (ASC; Jacobs, 1986), which flows westward around the Antarctic continent. The meridional slope of the front, together with tides and eddies (Stewart et al., 2019), regulates the strength of the ASC, but also the accessibility of the CDW to the continental shelf. A relaxed, relatively flattened ASF means that CDW is found higher up in the water column and is more likely to enter the shelf. The dynamics of the ASF/ASC system thus largely determine the on-shelf oceanic heat flux and, ultimately, the amount of heat reaching the cavities beneath the floating ice shelves fringing the Antarctic Ice Sheet (Heywood et al., 2014). Where the slope of the ASF is gentle, for example in the Amundsen Sea, the continental shelves and the ice shelf cavities are flooded with CDW, and basal melt rates are high (e.g. Pritchard et al., 2012; Rignot et al., 2013; Shepherd et al., 2018). The steeper ASF in the southern Weddell Sea, on the other hand, causes the thermocline (i.e. the interface between the Warm Deep Water (WDW), which is a slightly cooler and fresher version of CDW specific to the Weddell Sea and the colder Winter Water above) to incrop at the continental slope below the depth of the shelf break. The WDW hence has limited access to the Weddell shelf but is channeled southward along the flanks of the Filchner Trough (Ryan et al., 2017; Darelius et al., 2016, , see Fig. 1 for location) and the Central Trough west of the Berkner Bank (at 44°W, Nicholls et al., 2008). The WDW inflow occurs particularly during summer when the ASF relaxes, and WDW reaches higher up in the water column (Årthun et al., 2012; Semper & Darelius, 2017).

The waters of the wide continental shelf and the Filchner-Ronne ice shelf (FRIS) cavity are, in general, characterized by temperatures close to or below the surface freezing point (Nicholls et al., 2009), resulting in relatively low melt rates beneath FRIS. Future projections suggest a potential regime shift in the southern Weddell Sea, with WDW flooding the continental shelf and a dramatic increase in basal melt rates beneath the Filchner-Ronne Ice Shelf (FRIS). The shift is predicted to occur within this century (Hellmer

et al., 2012, 2017) or possibly beyond 2100 (Naughten et al., 2021; Nissen et al., 2022), and it would require a combination of changes in the thermocline depth over the continental slope and a reduction in the density of the cold and dense Ice Shelf Water (ISW), which currently prevents WDW from accessing the Filchner Trough and the FRIS cavity (K. Daae et al., 2020). The impact of increased melting beneath FRIS on the acceleration and thinning of the upstream ice sheet and the global sea level rise is debated (Hill et al., 2021) as the models used for these predictions are poorly constrained by observations. Paleo-records and simulations, however, point to the southern Weddell Sea and the Recovery basin as a region sensitive to change (Stokes et al., 2022). To better predict the likelihood and timing of a regime shift, we must understand the dynamics controlling the flow of WDW across the shelf break in the southern Weddell Sea. That is, we need to improve our understanding of the local ASC / ASF system.

Most of the observations of the westward-flowing ASC in the Weddell Sea are from the eastern Weddell Sea, where the continental shelf is narrow and the ASC/ASF is near the ice fronts. In this area, the ASC is merged with the coastal current, which follows the coastline and ice fronts around Antarctica (Heywood et al., 1998). The ASC is surface intensified (Heywood et al., 1998; Chavanne et al., 2010) with annual mean core velocities off Kapp Norvegia ranging from 10 to 20 cm/s (Fahrbach et al., 1992, , see Fig. 1 for location). It displays a relatively strong seasonal variation, reaching its maximum strength in autumn (Fahrbach et al., 1992; Nunez-Riboni & Fahrbach, 2009). This seasonal pattern appears coherent along the southern rim of the Weddell Sea (Le Pailh et al., 2020). The surface-intensified current weakens with increasing depth due to the southward-sloping isopycnals. In the eastern Weddell Sea, there are observations of an eastward undercurrent at deeper levels (Heywood et al., 1998; Smedsrud et al., 2006; Nunez-Riboni & Fahrbach, 2009; Chavanne et al., 2010). Near the seafloor, however, the tilt of the isopycnals often reverses, i.e., the isopycnals shoal towards the coast, potentially due to bottom Ekman transport (Smedsrud et al., 2006) and/or eddy overturning (Nøst et al., 2011; Hattermann et al., 2014; Stewart & Thompson, 2015).

Further west, the ASC separates from the coast and the coastal current near 27°W (Foster & Carmack, 1976), where the continental shelf widens. In this region, the presence of relatively dense water masses on the continental shelf gives rise to a V-shaped pycnocline (Gill, 1973; Thompson et al., 2018) that is co-located with the shelf break. Consequently, descriptions of ASC properties and variability based on observations from

the eastern Weddell Sea may not directly apply to the Filchner Trough region - a region identified as central for both the inflow of WDW (Ryan et al., 2017; Hellmer et al., 2012) and the outflow of dense ISW and the formation of Antarctic bottom water (Foldvik et al., 2004). Observations from 2021 suggest an unprecedented (in observations) warming of the WDW core above the upper part of the continental slope, accompanied by a freshening of the overlying Winter Water to the north of the Filchner Trough (Darelius et al., 2023). Although this warming does not appear to have propagated onto the continental shelf, where the inflow was warmer and stronger in 2017-2018 (Ryan et al., 2020), it highlights the need to improve our understanding of the dynamics and variability of the ASC/ASF system.

In this study, we describe the mean properties and the seasonality of the ASC/ASF and the hydrography on the upper continental slope just east of the Filchner Trough. Our analysis is based on a dataset spanning four years, from 2017 to 2021, obtained from oceanographic moorings deployed at depths of 530, 740, and 2570 m. We make use of (i) two neighboring continental slope moorings to quantify the slope of the isotherms/isopycnals in the vicinity of the shelf break and (ii) the length of the records to describe the average seasonal patterns and to identify links between the strength of the ASC and temperature anomalies. We use hydrographic data from ships and instrumented Weddell seals to discuss the broader context.

2 Data and methods

2.1 Mooring data

We analyze results from three oceanographic moorings, operated on the continental slope in the region east of Filchner Trough (Fig. 1) from 2017-2021. The moorings were deployed during the WAPITI cruise (JCR16004, Sallée, 2017) in February 2017 and recovered in February 2021 during the COSMUS expedition (PS124 Hellmer & Holtappels, 2021). The mooring data are available from Darelus (2023). Two moorings were deployed on the upper part of the slope: M₇₄₀ (74°33.00' S, 29°54.48' W) at 740 m depth and M₅₃₀ (74°35.70' S, 29°54.97' W) at 530 m depth. These moorings were equipped with current meters: 75 kHz (2 h) and 150 kHz (1h) Acoustic Doppler Current Profilers from RDI, Recording Current Meters from Aanderaa (2h), and hydrographic sensors: SBE37(600 s), SBE39(900 s), and SBE56(120 s) from Seabird Electronics (SBE), where the number in parenthesis gives the maximum sampling interval used for that instrument type (see Table 1 and Fig. 2). The third mooring, M₂₅₇₀ (74° 1.17' S, 28° 4.78' W) at 2750 m depth, was deployed to hold a sound source (for Argo positioning) but included two temperature sensors (one SBE39 and one SBE56, Table 1). Additionally, one-year-long records from a mooring deployed at approximately the M₇₄₀ position in 2009 (Jensen et al., 2013) complement the study.

The data from M₇₄₀ and M₅₃₀ were processed as described in Darelus (2023). If not stated otherwise, analyses are performed using records of hourly mean values (bi-hourly records are interpolated linearly). The alongslope current is obtained by rotating the coordinate system 146° counterclockwise, which roughly aligns the x -axis with the mean current at 300 mab. Moorings M₅₃₀ and M₇₄₀ are separated by 5 km, and M₂₅₇₀ is located 80 km from M₇₄₀. We assume that the measurements are de-correlated on the timescale of passing weather systems and continental shelf waves (about a week), and estimate the effective degrees of freedom (DOF) by the number of observations divided by the number of hours in a week, and the standard error by the standard deviation divided by the square root of DOF.

For comparison, data from moorings deployed between 2014 and 2021 at 76°S on the continental shelf east of the FT (CS, Ryan et al., 2017, cyan squares in Fig. 1) are discussed in the text.

Table 1. Details about moorings and mooring instrumentation. Depths with sensors for temperature and salinity are given in bold, and depths with only temperature are given in normal font. Ranges for velocity measurements with ADCP are given as shallowest bin : bin size : deepest bin.

¹ Point measurement

	Position	Period	Bottom depth [m]	Depth of hydrography sensors [m]	Depth of velocity bins [m]
M ₅₃₀	74°35.70' S, 29°54.97' W	2017-2021	530	505, 496 , 471, 456, 431 , 404, 379, 354 , 328	26:8:298, 506 ¹
M ₇₄₀	74°33.00' S, 29°54.48' W	2017-2021	740	716, 707 , 682, 657, 632, 604 , 579, 554, 529 , 503, 478, 453, 428, 403, 378, 353, 328 , 303	46:16:478, 717 ¹
M ₂₅₇₀	74° 1.17' S, 28° 4.78' W	2017-2021	2570 2570	571, 371	

2.2 Auxiliary data

CTD profiles from the continental slope are available from the deployment in 2017 (2017; Sallée, 2017) and recovery (2021; Hellmer & Holtappels, 2021) cruises. The position of the CTD profiles included in the study is shown in Fig. 1.

In addition, we use CTD profiles collected by instrumented Weddell Seals (downloaded from MEOP, Treasure et al., 2017). Profiles from the study area are available from 2007 (Nicholls et al., 2008), 2009, 2011 (Årthun et al., 2012) and 2014 (Nachtsheim et al., 2019). We include 112 profiles from the continental slope area upstream of FT (30°45' W - 25°30' W), where the temperature indicates a thick WW layer ($\Theta < -1.8^\circ$ C at 150 m depth). The profiles are binned according to month (Feb, April, June) and isobaths (500-600m and 600-700m). The number of profiles varies with year and month, with a total of 30 profiles from February (21 from 2007 and 9 from 2009), 43 profiles from April (16 from 2007, 25 from 2011, and 2 from 2014), and 39 profiles from June (8 from 2007 and 31 from 2011).

Mooring records are compared to results extracted from the gridded monthly mean climatology compiled by Hattermann (2018) based on data from the region around Kapp Norvegia.

Monthly mean sea ice concentrations and zonal 10m-wind velocities are extracted from the ERA5 reanalysis (Hersbach et al., 2020) for the period 1979-2021 and averaged over the region 24-36°W, 73-75.5°S.

2.3 Isotherm slope and the relation between temperature and density

To quantify the slope of the isotherms between the two moorings on the upper part of the continental slope, we define

$$\Delta ITD(\theta, t) = ITD(\theta, t)_{M_{740}} - ITD(\theta, t)_{M_{530}} \quad (1)$$

where $ITD(\theta, t)_{M_X}$ is the depth of the isotherm θ , inferred through linear interpolation (in the vertical, resolution 5m) at each time step at mooring M_X . $\Delta ITD(\theta, t)$ is calculated only when the isotherm was captured in both M_{740} and M_{530} .

At the depths covered by M_{530} and M_{740} and within the relevant temperature range (-1.5°C–0.4°C), the density anomaly (referenced to 600 m) can be approximated (using the CTD-data and linear regression) from the Conservative Temperature, Θ , as

$$\sigma_{600} = 0.037\Theta + 30.6 \quad (2)$$

As a result, isopycnals are parallel to isotherms, and a positive ΔITD means that isotherms and isopycnals slope upward towards the shelfbreak.

3 Results

Moorings M_{530} and M_{740} were deployed at the upper part of the continental slope, separated by about 5 km. The shallow part of the moorings is surrounded by relatively cold and fresh Winter Water (WW), while the deeper part of the moorings is (mostly) surrounded by warm mWDW (Fig. 2), and the moorings hence typically capture the thermocline and the upper part of the WDW-layer. There is large variability in thermocline depth on daily timescales caused by continental shelf waves that move the thermocline more than 100 m vertically as they travel past the moorings (Jensen et al., 2013; Semper & Darelius, 2017). Variability on shorter time scales in the records will be discussed elsewhere. We note that when the tides (which are relatively strong and enhanced sea-

sonally by resonant shelf waves Semper & Darelius, 2017) are filtered out, the current is directed westward along the slope, and that it is quasi-unidirectional (Fig. 3c-d). In this study, we use the 4-year records to investigate mean conditions and specifically focus on the seasonal variability of the ASF/ASC characteristics.

3.1 Mean conditions

The moorings are located within the ASC, and the mean current is directed westward along the isobaths (Fig. 1 and Fig. 4) with mean velocities on the order of 0.10 m s^{-1} . The upper instruments (above 350 m) of the moorings are surrounded by cold ($\Theta \simeq -1.9^\circ\text{C}$) water, and temperatures increase monotonically towards the bottom where they reach -0.4°C and -1.1°C at M_{740} and M_{530} , respectively. The highest temperatures (above 0.7°C) are found towards the end of the records (Darelius et al., 2023).

The time-averaged, vertical current profiles (Fig. 4a,c) reveal that the current on both moorings is bottom-enhanced. The mean velocity increases by about 50% over the bottom-most 200 m, i.e. roughly over the depth of the layer that is influenced by mWDW. The temperature profiles (Fig. 4b), on the other hand, show that the temperature at a given depth is higher on M_{530} than at M_{74} . This means that warm, dense (see Sec. 2.3) mWDW shoals towards the shelf break. The upward-sloping isotherms are also apparent in the temperature sections from the deployment cruise (Fig. 2a). The difference in isotherm depth between the two moorings, ΔITD (eq. 1), is hence on average positive. The distribution of ΔITD consistently shifts towards higher values (i.e., steeper isotherm slope) for higher temperatures (Fig. 5a). For water warmer than 0°C the time-averaged value of ΔITD is above 150 m. This is consistent with a bottom-enhanced westward flow in thermal wind balance. The velocity at the bottom at both M_{740} and M_{530} is higher for higher values of ΔITD (not shown), and the vertical velocity shear in the lower part of the water column is larger when the temperature at the bottom is high (Fig. 5b).

3.2 Seasonal variability

The seasonal variability in the region is, in general, large. As summer transitions to winter, the daylight disappears, the temperature drops and the sea ice cover builds up and reaches close to 100% (Fig. 6a). The seasonal freeze-melt cycle and a seasonally variable momentum transfer from the atmosphere induce seasonal changes in the upper

ocean hydrography, which further affects the ASF/ASC system and modulates the inflow of mWDW onto the continental shelf east of the FT (Årthun et al., 2012; Ryan et al., 2017). While the local seasonal signal in the wind forcing is weak (Fig. 6a), it has been shown that the ASC upstream of the study area is forced remotely (Lauber, Hattermann, et al., 2023; Le Paih et al., 2020). To describe the mean seasonality in the region, we use the 4-year-long time series to generate seasonal climatology with monthly resolution.

The temperature climatology confirms the seasonal change in thermocline depth above the continental slope in the region apparent in Fig. 3a-b and described by, e.g. Semper and Darelius (2017). The mean position of the thermocline at M₇₄₀ is about 200 m shallower during austral summer than during winter. The seasonality in thermocline depth is asymmetric, with a relatively abrupt drop in March-April (most clearly seen in Fig. 3a as interannual variability in the timing smears the signal out in Fig. 6b-c) and a more progressive shoaling during winter and spring.

The mean bottom temperature is accordingly the highest towards the end of austral summer when it reaches close to 0°C. It is, on average, about 1°C lower during winter (Fig. 6b-c). The hydrographic changes in the lower part of the water column follow the mixing line between WDW and WW (Fig. 2b, triangles), suggesting that they result from the heaving and sinking of the WDW-WW interface, and not from e.g. advection. Higher up in the water column, the temperature remains at or close to the surface freezing point (-1.9°C) throughout the year, while the salinity varies. The absolute salinity at M₇₄₀, 328 m depth, is about 0.1 g kg⁻¹ higher during summer than in winter (Fig. 2b, squares, and 6d). At M₅₃₀ (354 m depth), the phasing of the seasonality in salinity is similar, but since the amplitude is slightly lower, the difference in salinity between the two moorings is largest during winter (JJA) and smallest in autumn and spring.

The seasonal changes in hydrography are accompanied by seasonality in the strength of the along-slope current, which is strongest (0.20-0.25 m s⁻¹) at the bottom of M₇₄₀ and M₅₃₀) in autumn and weakest (<0.10 m s⁻¹) in spring (Fig. 6e). The current above the upper part of the slope hence increases when the thermocline is deepening and the temperatures above the slope decrease, and the current is weak when the thermocline is shoaling and temperatures increase. This is consistent with a barotropic, along-slope current driven by Ekman convergence along the coast. As surface water piles up along the coast, the current strength increases rapidly, and the thermocline depth decreases.

While interannual variability of the ASC, its cause, and effect on the mWDW in-flow and the hydrography on the continental shelf are discussed by Steiger (2023), we note here that the link between weak currents and high temperatures, established above on a seasonal scale, also holds on interannual time scales. When we subtract the mean seasonal signal from records of monthly mean temperature and along-slope velocity, Fig. 11, a consistent pattern of interannual variability appears; temperatures are generally above average for the first and last part of the record, and below average in the middle part of the record. The along-slope velocity shows the opposite pattern, with velocities less than average in the first and last parts of the record. Over the full record, temperature and current anomalies are negatively correlated (typically $r \simeq -0.5$ at mid-level on M_{740} , significant at 95% level following (Sciremammano, 1979)) with the maximum correlation occurring at one month lag (current leads). The correlation is lower (typically $r \simeq -0.4$ and barely significant at 95%-level) at M_{530} .

Returning to the current measurements from M_{530} and M_{740} , we note that it is not only the strength but also the vertical structure of the current that changes throughout the year (Fig. 7). The vertical shear in the shallower part of the records (above 200 mab and typically within the WW-layer) and that of the lower part of the water column (affected by mWDW) evolves differently throughout the year. To highlight the difference in the seasonal evolution of the vertical shear, we show the monthly mean "bulk" gradient, $\Delta u / \Delta z$ of the two layers in Fig. 9 and compare the results to the observed horizontal density gradients (using the equations for thermal wind balance) and seasonal changes in ΔITD (Fig. 8).

The currents in the portion of the water column that is more than 200 mab show little change with depth during most of the year (August - March/April), while gradients are relatively large during the winter months. The currents then increase with depth throughout most of the (observed) water column. The thermal wind balance tells us that the density hence must be increasing towards the south. Indeed, CTD-profiles collected by instrumented Weddell Seals in the area during winter suggest that salinities in the upper part of the water columns are higher over shallower isobaths (Fig. 10). The observed shear (above 200 mab) is largest at M_{530} , but this is partly an artifact of the analysis, as the small depth range with data return during austral summer at M_{740} limits the depth range over which the velocity gradient in Fig. 9a is calculated. The vertical gradients are weaker and close to zero during spring and summer, especially at M_{530} . The

magnitude of the vertical gradient over the upper layer agrees with thermal wind estimates using the observed horizontal density gradient (Fig. 9a,c).

We saw above that the bottom enhancement is - at least partly - associated with mWDW "climbing" up along the bottom and upward-sloping isotherms, but although there is a tendency for higher values of ΔITD during winter (Fig. 8) there is no apparent seasonal signal in the vertical velocity shear for the lower part of the water column (Fig. 9b).

Finally, we note that the seasonal signal in temperature observed at M₂₅₇₀, located 80 km to the northeast of M₇₄₀, above the 2570 m isobath, is out of phase with the observations from M₇₄₀ and M₅₃₀; when the temperature drops above the upper part of the continental slope as the mWDW deepens, the temperature at M₂₅₇₀ increases, suggesting that the mWDW *rises* above the deeper part of the slope (Fig. 6f). A similar temperature maximum in March-April is observed at similar depths in the monthly climatology from Kapp Norvegia (Hattermann, 2018) above the deeper part of the slope (Fig. 6f, but these records all show an additional, secondary temperature maximum in December-January. Lauber, de Steur, et al. (2023) show similar out-of-phase behavior in thermocline depth between shallow and deep isobaths just east of the Fimbul ice shelf (around the 0°W).

4 Discussion

New observations spanning the period 2017-2021 from two moorings on the upper part of the continental slope just east of the Filchner Trough reveal details of the structure, seasonality, and interannual variability of the ASC/ASF at the southern Weddell Sea continental slope. The study area is on the border between the "Fresh shelf/Surface intensified ASC" in the east and the "Dense shelf/Bottom intensified ASC" further west (Huneke et al., 2022; Thompson et al., 2018). The westward flowing current is bottom enhanced, in agreement with the modeled results by Huneke et al. (2022), but contrary to their results, the current shows a strong seasonal signal also at depth; the current is strongest during April-June when monthly mean currents reach a strength of 0.25 (0.15) m s⁻¹ at 25 (250) mab.

The vertical shear is largest when the current is strongest in April-June. This is due to an on-shore directed salinity gradient in the upper layer. The monthly mean along-slope velocities in April-June are 0.1-0.2 m s⁻¹ larger than the minimum velocity, which

is recorded in September-October. The amplitude of seasonal variability in the along-slope current is larger at the bottom than higher up in the water column and larger over shallower isobaths (M_{530}) than over deeper isobaths (M_{750}). The timing of the maximum velocities in late autumn observed at M_{530} and M_{750} align with maximum ASC transport inferred at 17°W (Graham et al., 2013) and with maximum velocities reported from the Prime Meridian and Kapp Norvegia ($0 / 12^\circ\text{W}$, Le Paih et al., 2020). We note, however, that the seasonal amplitude in M_{530} and M_{750} is larger by a factor of at least two (compared to Le Paih et al., 2020; Auger et al., 2022).

The thermocline depth shows a pronounced seasonal cycle (Årthun et al., 2012; Semper & Darelius, 2017), with a vertical excursion of about 200 m in its (monthly) mean position. This vertical excursion in the monthly averaged records is distinct from excursions of similar amplitude on daily timescales caused by coastal trapped waves (Jensen et al., 2013). The thermocline is at its shallowest towards the end of the summer (February), and it then drops rapidly in Autumn (March - April) when the mWDW more or less completely disappears from M_{530} .

The seasonal inflow of mWDW onto the continental shelf east of the FT (Årthun et al., 2012; Ryan et al., 2017) occasionally reaches the Filchner ice front (Darelius et al., 2016), and it is tightly linked to the seasonality above the slope. The thermocline deepens in March-April and shuts off the warm inflow, as mWDW is no longer available at depths shallower than the depth of the shelf break (Ryan et al., 2017). The prolonged warm inflow in 2017 (Ryan et al., 2020), during which warmer than usual mWDW was surrounding oceanographic moorings on the shelf (76°S , see Fig. 1) several months longer than in the rest of the record (Ryan et al., 2017; Steiger, 2023), does, however, not seem to be caused by a prolonged warm situation on the shelf break. While water during the inflow season of 2017 is warmer than "normal" (Fig. 11), the warm water disappears from the upper part of the slope in April "as usual" (Fig. 3b) and winter temperatures in 2017 at $M_{530/740}$ were not anomalously high.

We note that the period during which actual inflow, i.e., southward flow, is observed at 76°S (Ryan et al., 2017, their "phase 2" (roughly April-June), see their Fig. 3) coincides with the period of maximum current strength at M_{530} and M_{750} (Fig. 6d). The advection time scale from the shelf break to 76°S is on the order of several weeks or months (Steiger, 2023), and since the mWDW appears at the 76°S mooring sites before or immediately after the currents here shift to a southward direction, there must have been

southward flow on the continental shelf further north earlier in the season. One plausible explanation, consistent with the observations, is that a circulation cell on the shelf east of the FT, which includes a southward flow (of mWDW, when present) and a northward return flow above the eastern flank of the FT, extends further south in the period when the current over the shelf break is strongest.

Easterly winds and converging Ekman transports along the coast generally cause a southward deepening of the thermocline (Sverdrup, 1953), but the mooring records show a persistent upward slope of isotherms (and hence isopycnals) towards the shelf break. Isotherms sloping upwards towards the shelf break are regularly observed above the continental slope in CTD sections from the southern Weddell Sea (Chavanne et al., 2010; Nøst, 2004; Heywood et al., 1998, and Fig. 2). The uplift could potentially facilitate the on-shelf flow of warm water as mWDW is lifted to shallower depths - but the uplift is largest during winter when the warm inflow is limited (Fig. 5c). Nøst et al. (2011) suggest that one potential explanation for the shoaling isotherms (isopycnals) is the interaction between eddies and a sloping topography (Greatbatch & Li, 2000). We note, however, that the Eddy Kinetic Energy (EKE) in the region shows a pronounced maximum during summer (Darelius et al., 2023, , their Fig. 6), whereas the uplift is largest during winter.

It is also possible that the presence of the FT is causing or contributing to the southward thermocline shoaling, as water columns are steered onto shallower isobaths to conserve potential vorticity when encountering the "corner" (i.e., the southward bending isobaths) of the FT opening (Williams et al., 2001). To further investigate this effect, we apply the scaling for the radius of curvature, R_c , suggested by Williams et al. (2001) to a barotropic shelf break jet over a sloping bottom that encounters a sharp corner:

$$R_c = 1.3 \sqrt{\frac{U h_0}{f \nabla h}} \quad (3)$$

where U is the along slope velocity, h_0 the initial depth of the stream line considered, $f = 10^{-4} \text{ s}^{-1}$ the Coriolis parameter and $\nabla h \simeq \Delta h / \Delta x \simeq 0.04$ at the mooring site. If the shear of the jet is small compared to f and we assume that changes in the shape of the jet as it moves around the corner can be ignored (in Williams et al. (2001) simulations, this largely holds above the slope but not on the shelf), then conservation of potential vorticity gives

$$\frac{f}{h_0} = \frac{f - U/R_c}{h_0 - \Delta h} \quad (4)$$

and we can solve for $\Delta h = F(U, \nabla h, h_0)$, where Δh is the change in depth of a water column needed to compensate for the change in potential vorticity of the turning jet. Δh increases for increasing values of U , h_0 , and ∇h (Fig. 12a) and are on the order of 100–200m for values relevant to our mooring site. If the entire jet moves onto shallower isobaths, then the depth of a given isotherm D_0 would decrease so that $D'_0 = D_0/h_0x(h_0 - \Delta h)$, and since the effect is larger over shallower isobaths, this gives rise to upward sloping isotherms (Fig. 12b). The scaling suggests that the effect could be noticeable at the mooring site and that it, in accordance with the observations, would increase with increasing velocities. Note, however, that the results and the scaling by Williams et al. (2001) are valid for a barotropic jet and a case where all isobaths make a corner, whereas, on the mooring site, the current has a baroclinic component (Fig. 7) and only the shallower isobaths turn into the Filchner Trough. A similar behavior, with streamlines "cutting the corner" to conserve potential vorticity, is, however, observed also in Williams et al. (2001)'s trough simulations, which largely resembles the setting at the Filchner Trough (albeit barotropic and in the northern hemisphere). It is not clear how stratification and the baroclinic component of the flow would affect the results.

5 Summary

We have described the mean properties and the seasonal signal of the ASC/ASF system above the upper part of the slope just east of the Filchner Trough based on new, four-year-long mooring records. In this region, the ASC close to the shelf break has a mean strength of about 0.1 m s^{-1} , and the current is bottom-enhanced. The vertical shear in the upper part of the water column is largest during austral winter when the horizontal salinity gradient between the relatively dense shelf and the fresher waters of the ASC is largest. The isotherms in the lower part of the water column shoal towards the shelf break, and since the isotherms are parallel to isopycnals, the tilt contributes to the bottom enhancement of the current. Maximum isotherm tilt is observed during winter, and it is larger for higher temperatures and stronger currents. We suggest that the shoaling is linked to local topography and the conservation of potential vorticity. As the ASC encounters the southward turning isobaths marking the opening of the FT, it climbs higher up on the slope to compensate for the potential vorticity induced by the curved streamlines.

The mooring records reveal a strong seasonality in the ASC/ASF system, with the highest along-slope velocities in April-June and the highest temperatures / shallowest thermocline in February-March. Anomalously strong currents appear to be connected to negative temperature anomalies at one month lag.

Further observational and modeling studies are needed to understand the link between atmospheric forcing, the strength of the ASC / ASF and the inflow of warm water towards the ice shelf cavities.

Acknowledgements

This work was funded by the Norwegian Research Council, projects 267660, 328941, and 295075. The moorings were recovered during the COSMUS expedition (PS124). NS received funding from the European Union's Horizon 2020 research and innovation program under grant agreement N°821001 (SO-CHIC).

References

- Årthun, M., Nicholls, K. W., Makinson, K., Fedak, M. A., & Boehme, L. (2012, 9). Seasonal inflow of warm water onto the southern Weddell Sea continental shelf, Antarctica. *Geophysical Research Letters*, 39(17), L17601. doi: 10.1029/2012GL052856
- Auger, M., Sallée, J. B., Prandi, P., & Naveira Garabato, A. C. (2022). Subpolar Southern Ocean Seasonal Variability of the Geostrophic Circulation From Multi-Mission Satellite Altimetry. *Journal of Geophysical Research: Oceans*, 127(6). doi: 10.1029/2021JC018096
- Chavanne, C. P., Heywood, K. J., Nicholls, K. W., & Fer, I. (2010, 7). Observations of the Antarctic Slope Undercurrent in the southeastern Weddell Sea. *Geophysical Research Letters*, 37(13), n/a-n/a. Retrieved from <http://doi.wiley.com/10.1029/2010GL043603> doi: 10.1029/2010GL043603
- Daae, K., Hattermann, T., Darelius, E., Mueller, R. D., Naughten, K. A., Timmermann, R., & Hellmer, H. H. (2020). Necessary Conditions for Warm Inflow Towards the Filchner Ice Shelf, Weddell Sea. *Geophysical Research Letters*, 47. Retrieved from <https://onlinelibrary.wiley.com/doi/10.1029/2020GL089237> doi: 10.1029/2020GL089237
- Daae, K. B., Hattermann, T., Darelius, E., & Fer, I. (2017). On the effect of to-

- 438 pography and wind on warm water inflow - An idealized study of the southern
 439 Weddell Sea continental shelf system. *Journal of Geophysical Research :
 440 Oceans*, 122, 2017–2033. doi: 10.1002/2016JC012541
- 441 Darelius, E. (2023). *Data processing: M3, Southern Weddell Sea 2017-2021*. PAN-
 442 GAEA. Retrieved from <https://doi.pangaea.de/10.1594/PANGAEA.962043>
- 443 Darelius, E., Dundas, V., Janout, M. A., & Tippenhauer, S. (2023). Sudden, local
 444 temperature increase above the continental slope in the Southern Weddell Sea,
 445 Antarctica. *Ocean Science*. doi: 10.5194/os-19-671-2023
- 446 Darelius, E., Fer, I., & Nicholls, K. W. (2016). Observed vulnerability of Filchner-
 447 Ronne Ice Shelf to wind-driven inflow of warm deep water. *Nature Communi-
 448 cations*, 7:12300. doi: 10.1038/ncomms12300
- 449 Darelius, E., Makinson, K., Daae, K., Fer, I., Holland, P. R., & Nicholls, K. W.
 450 (2014). Circulation and hydrography in the Filchner Depression. *Journal of
 451 Geophysical Research*, 119, 1–18. doi: 10.1002/2014JC010225
- 452 Fahrbach, E., Rohardt, G., & Krause, G. (1992). The {A}ntarctic {C}oastal
 453 {C}urrent in the southeastern {W}eddell {S}ea. *Polar Biology*, 12, 171–182.
- 454 Foldvik, A., Gammelsrød, T., Østerhus, S., Fahrbach, E., Rohardt, G., Schröder, M.,
 455 ... Woodgate, R. A. (2004). Ice shelf water overflow and bottom water for-
 456 mation in the southern Weddell Sea. *Journal of Geophysical Research-Oceans*,
 457 109(C2). doi: 10.1029/2003JC002008
- 458 Foster, T. D., & Carmack, E. C. (1976). Frontal zone mixing and Antarctic Bottom
 459 Water formation in the southern Weddell Sea. *Deep Sea Research*, 23(March
 460 1975), 301–317.
- 461 Fretwell, P., Pritchard, H. D., Vaughan, D. G., Bamber, J. L., Barrand, N. E.,
 462 Bell, R., ... Zirizzotti, A. (2013, 2). Bedmap2: Improved ice bed, sur-
 463 face and thickness datasets for Antarctica. *Cryosphere*, 7(1), 375–393. doi:
 464 10.5194/tc-7-375-2013
- 465 Gill, A. E. (1973). Circulation and bottom water production in the Weddell Sea.
 466 *Deep-Sea Research*, 20, 111–140.
- 467 Graham, J. A., Heywood, K. J., Chavanne, C. P., & Holland, P. R. (2013, 4). Sea-
 468 sonal variability of water masses and transport on the Antarctic continental
 469 shelf and slope in the southeastern Weddell Sea. *Journal of Geophysical Re-
 470 search: Oceans*, 118(4), 2201–2214. doi: 10.1002/jgrc.20174

- Greatbatch, R. J., & Li, G. (2000). Alongslope mean flow and an associated upslope bolus flux of tracer in a parameterization of mesoscale turbulence. *Deep-Sea Research Part I: Oceanographic Research Papers*, 47(4), 709–735. doi: 10.1016/S0967-0637(99)00078-3
- Hattermann, T. (2018). Antarctic thermocline dynamics along a narrow shelf with easterly winds. *Journal of Physical Oceanography*, 18–0064. Retrieved from <http://journals.ametsoc.org/doi/10.1175/JPO-D-18-0064.1> doi: 10.1175/JPO-D-18-0064.1
- Hattermann, T., Smedsrud, L. H., Nøst, O. A., Lilly, J., & Galton-Fenzi, B. (2014, 8). Eddy-resolving simulations of the Fimbul Ice Shelf cavity circulation: Basal melting and exchange with open ocean. *Ocean Modelling*. doi: 10.1016/j.ocemod.2014.07.004
- Hellmer, H. H., & Holtappels, M. (2021). *The Expedition PS124 of the Research Vessel Polarstern to the southern Weddell Sea in 2021* (Tech. Rep.). Bremerhafen: Alfred Wegner Institute for Polar and Marine Research. doi: 10.48433/BzPM{\-}0755{\-}2021
- Hellmer, H. H., Kauker, F., Timmermann, R., Determann, J., & Rae, J. (2012, 5). Twenty-first-century warming of a large Antarctic ice-shelf cavity by a redirected coastal current. *Nature*, 485(7397), 225–228. doi: 10.1038/nature11064
- Hellmer, H. H., Kauker, F., Timmermann, R., Hattermann, T., Shelf, F.-r. I., & Mengel, M. (2017). The fate of the southern Weddell Sea continental shelf in a warming climate. *Journal of Climate*, 30. doi: 10.1175/JCLI-D-16-0420.1
- Hersbach, H., Bell, B., Berrisford, P., Hirahara, S., Horányi, A., Muñoz-Sabater, J., ... Thépaut, J. N. (2020). The ERA5 global reanalysis. *Quarterly Journal of the Royal Meteorological Society*, 146(730), 1999–2049. doi: 10.1002/qj.3803
- Heywood, K. J., Locarnini, R. A., Frew, R. D., Dennis, P. F., & King, B. A. (1998). Transport and water masses of the Antarctic Slope Front system in the eastern Weddell Sea. In S. S. Jacobs & R. Weiss (Eds.), *Ocean, ice, and atmosphere - interaction at the antarctic continental margin* (75th ed., Vol. 75, pp. 203–214). Washington D. C.: American Geophysical Union. Retrieved from <http://www.agu.org/books/ar/v075/AR075p0203/AR075p0203.shtml> doi: doi:10.1029/AR075p0203
- Heywood, K. J., Schmidtke, S., Heuzé, C., Kaiser, J., Jickells, T. D., Queste, B. Y.,

- ... Smith, W. (2014). Ocean processes at the Antarctic continental slope. *Philosophical Transactions of the Royal Society A: Mathematical, Physical and Engineering Sciences*, 372(2019). doi: 10.1098/rsta.2013.0047
- Hill, E. A., Rosier, S. H. R., Gudmundsson, G. H., & Collins, M. (2021). Quantifying the potential future contribution to global mean sea level from the Filchner-Ronne basin, Antarctica. *The Cryosphere Discussions*(April), 1–43. doi: 10.5194/tc-2021-120
- Huneke, W. G., Morrison, A. K., & Hogg, A. M. (2022). Spatial and Subannual Variability of the Antarctic Slope Current in an Eddy Ocean–Sea Ice Model. *Journal of Physical Oceanography*, 52(3), 347–361. doi: 10.1175/JPO-D-21-0143.1
- Jacobs, S. S. (1986). The Antarctic Slope Front. *Antarctic Journal of the United States*, 21, 123–124.
- Jensen, M. F., Fer, I., & Darelius, E. (2013, 7). Low frequency variability on the continental slope of the southern Weddell Sea. *Journal of Geophysical Research: Oceans*, 118. doi: 10.1002/jgrc.20309
- Lauber, J., de Steur, L., Hattermann, T., & Darelius, E. (2023). Observed Seasonal Evolution of the Antarctic Slope Current System off the Coast of Dronning Maud Land, East Antarctica. *Journal of Geophysical Research (in revision)*. doi: 10.22541/essoar.169755155.52018682/v1
- Lauber, J., Hattermann, T., de Steur, L., Darelius, E., Auger, M., Nøst, O. A., & Moholdt, G. (2023). Warming beneath an East Antarctic ice shelf due to increased subpolar westerlies and reduced sea ice. *Nature Geoscience*, 16(October). Retrieved from <https://www.nature.com/articles/s41561-023-01273-5> doi: 10.1038/s41561-023-01273-5
- Le Paih, N., Hattermann, T., Boebel, O., Kanzow, T., Lüpkes, C., Rohardt, G., ... Herbet, S. (2020). Coherent Seasonal Acceleration of the Weddell Sea Boundary Current System Driven by Upstream Winds. *Journal of Geophysical Research: Oceans*, 125(10), 1–20. Retrieved from <https://doi.org/10.1029/2020JC016316> doi: 10.1029/2020JC016316
- Nachtsheim, D. A., Ryan, S., Schröder, M., Jensen, L., Oosthuizen, W. C., Bester, M. N., ... Bornemann, H. (2019). Foraging behaviour of Weddell seals (*Leptonychotes weddellii*) in connection to oceanographic conditions in the

- southern Weddell Sea. *Progress in Oceanography*, 173(April 2018), 165–179.
Retrieved from <https://doi.org/10.1016/j.pocean.2019.02.013> doi:
10.1016/j.pocean.2019.02.013
- Naughten, K. A., De Rydt, J., Rosier, S. H., Jenkins, A., Holland, P. R., &
Ridley, J. K. (2021). Two-timescale response of a large Antarctic ice
shelf to climate change. *Nature Communications*, 12(1), 1–10. Re-
trieved from <http://dx.doi.org/10.1038/s41467-021-22259-0> doi:
10.1038/s41467-021-22259-0
- Nicholls, K. W., Boehme, L., Biuw, M., & Fedak, M. A. (2008). Wintertime ocean
conditions over the southern Weddell Sea continental shelf, Antarctica. *Geo-
physical Research Letters*, 35. doi: 10.1029/2008GL035742
- Nicholls, K. W., Østerhus, S., Makinson, K., Gammelsrød, T., & Fahrbach, E.
(2009). Ice-Ocean Processes over the Continental Shelf of the Southern
Weddell Sea, Antarctica: A Review. *Reviews of Geophysics*, 47, 1–23. doi:
10.1029/2007RG000250
- Nissen, C., Timmermann, R., Hoppema, M., Gürses, O., & Hauck, J. (2022).
Abruptly attenuated carbon sequestration with Weddell Sea dense waters
by 2100. *Nature Communications*, 13(1). doi: 10.1038/s41467-022-30671-3
- Nøst, O. A. (2004). Measurements of ice thickness and seabed topography under
the Fimbul Ice Shelf. *Journal of Geophysical Research : Oceans*, 109. Re-
trieved from [https://www.ptonline.com/articles/how-to-get-better-mfi-
results](https://www.ptonline.com/articles/how-to-get-better-mfi-results) doi: <https://doi.org/10.1029/2004JC002277>
- Nøst, O. A., Biuw, M., Tverberg, V., Lydersen, C., Hattermann, T., Zhou, Q., ...
Kovacs, K. M. (2011, 11). Eddy overturning of the Antarctic Slope Front
controls glacial melting in the Eastern Weddell Sea. *Journal of Geophysical
Research*, 116(C11), C11014. doi: 10.1029/2011JC006965
- Nunez-Riboni, I., & Fahrbach, E. (2009). Seasonal variability of the Antarctic
Coastal Current and its driving mechanisms in the Weddell Sea. *Deep-Sea
Research Part I-Oceanographic Research Papers*, 56(11), 1927–1941.
- Orsi, A. H., Smethie, W. M., & Bullister, J. L. (2002). On the total input of antarc-
tic waters to the deep ocean: a preliminary estimate from chlorofluorocar-
bon measurements. *Journal of Geophysical Research-Oceans*, 107(C8). doi:
10.1029/2001JC000976

- Pritchard, H. D., Ligtenberg, S. R. M., Fricker, H. A., Vaughan, D. G., Broeke, M. R. V. D., Padman, L., & van den Broeke, M. R. (2012, 4). Antarctic ice-sheet loss driven by basal melting of ice shelves. *Nature*, *484*(7395), 502–505. doi: 10.1038/nature10968
- Rignot, E., Jacobs, S. S., Mouginot, J., & Scheuchl, B. (2013, 7). Ice-shelf melting around Antarctica. *Science (New York, N.Y.)*, *341*(6143), 266–270. doi: 10.1126/science.1235798
- Ryan, S., Hattermann, T., Darelius, E., & Schröder, M. (2017). Seasonal Cycle of Hydrography on the Eastern Shelf of the Filchner Trough, Weddell Sea, Antarctica. *Journal Geophysical Research - Oceans*, *122*. doi: 10.1002/2017JC012916
- Ryan, S., Hellmer, H. H., Janout, M., Darelius, E., & Schröder, M. (2020). Exceptionally Warm and Prolonged Flow of Warm Deep Water toward the Filchner-Ronne Ice Shelf in 2017. *Geophysical Research Letters*, *47*, 1–24. doi: 10.1029/2020GL088119
- Sallée, J. B. (2017). *WAPITI cruise, RV JAMES CLARK ROSS* (Tech. Rep.). Retrieved from <https://campagnes.flotteoceanographique.fr/campagnes/18002130/> doi: 10.17600/18002130
- Sciremammano, F. J. (1979). A Suggestion for the Presentation of Correlations and Their Significance Levels. *Journal Of Physical Oceanography*, *9*, 1273–1276.
- Semper, S., & Darelius, E. (2017). Seasonal resonance of diurnal coastal trapped waves in the Weddell Sea, Antarctica. *Ocean Science*, *13*, 77–93. doi: 10.5194/os-13-77-2017
- Shepherd, A., Fricker, H. A., & Farrell, S. L. (2018). Trends and connections across the Antarctic cryosphere. *Nature*, *558*(7709), 223–232. doi: 10.1038/s41586-018-0171-6
- Smedsrud, L. H., Jenkins, A., Holland, D. M., & Nøst, O. A. (2006). Modeling ocean processes below Fimbulisen, Antarctica. *Journal of Geophysical Research*, *111*(C1), C01007. doi: 10.1029/2005JC002915
- Steiger, N. (2023). Observed pathways and variability of the WDW inflow in the Southern Weddell Sea. *Journal of Geophysical Research (submitted)*.
- Stewart, A. L., Klocker, A., & Menemenlis, D. (2019). Acceleration and Overturning of the Antarctic Slope Current by Winds, Eddies, and Tides. *Journal of Physi-*

- 603 *cal Oceanography*, 49(8), 2043–2074. doi: 10.1175/jpo-d-18-0221.1
- 604 Stewart, A. L., & Thompson, A. F. (2015). Eddy-mediated transport of warm Cir-
 605 cumpolar Deep Water across the Antarctic Shelf Break. *Geophys. Res. Lett.*,
 606 42, 432–440. doi: 10.1002/2014GL062281.1.
- 607 Stokes, C. R., Abram, N. J., Bentley, M. J., Edwards, T. L., England, M. H., Fop-
 608 pert, A., ... Paxman, G. J. G. (2022). Response of the East Antarctic Ice
 609 Sheet to past and future climate change. *Nature*, 608(April 2021). doi:
 610 10.1038/s41586-022-04946-0
- 611 Sverdrup, H. (1953). The currents off the coast of Queen Maud Land. *Norsk Ge-*
 612 *ografisk Tidsskrift*, 14(1), 239–249. doi: 10.1080/00291955308542731
- 613 Thompson, A. F., Stewart, A. L., Spence, P., & Heywood, K. J. (2018). The
 614 Antarctic Slope Current in a Changing Climate. *Reviews of Geophysics*.
 615 Retrieved from <http://doi.wiley.com/10.1029/2018RG000624> doi:
 616 10.1029/2018RG000624
- 617 Treasure, A. M., Roquet, F., Ansorge, I. J., Bester, M. N., Boehme, L., Bornemann,
 618 H., ... Nico De Bruyn, P. J. (2017). Marine mammals exploring the oceans
 619 pole to pole: A review of the meop consortium. *Oceanography*, 30(2), 132–138.
 620 doi: 10.5670/oceanog.2017.234
- 621 Whitworth, T., Orsi, A., Kim, S.-J., & Nowlin, W. D. (1998). Water Masses and
 622 Mixing near the Antarctic Slope Front. In S. S. Jacobs & R. F. Weiss (Eds.),
 623 *Ocean, ice, and atmosphere: Interactions at the antarctic continental margin*
 624 (Vol. 75, pp. 1–27). Washington, D.C.: American Geophysical Union.
- 625 Williams, W. J., Gawarkiewicz, G. G., & Beardsley, R. C. (2001). The adjustment of
 626 a shelfbreak jet to cross-shelf topography. *Deep-Sea Research Part II: Topical*
 627 *Studies in Oceanography*, 48(1-3), 373–393. doi: 10.1016/S0967-0645(00)00085
 628 -0

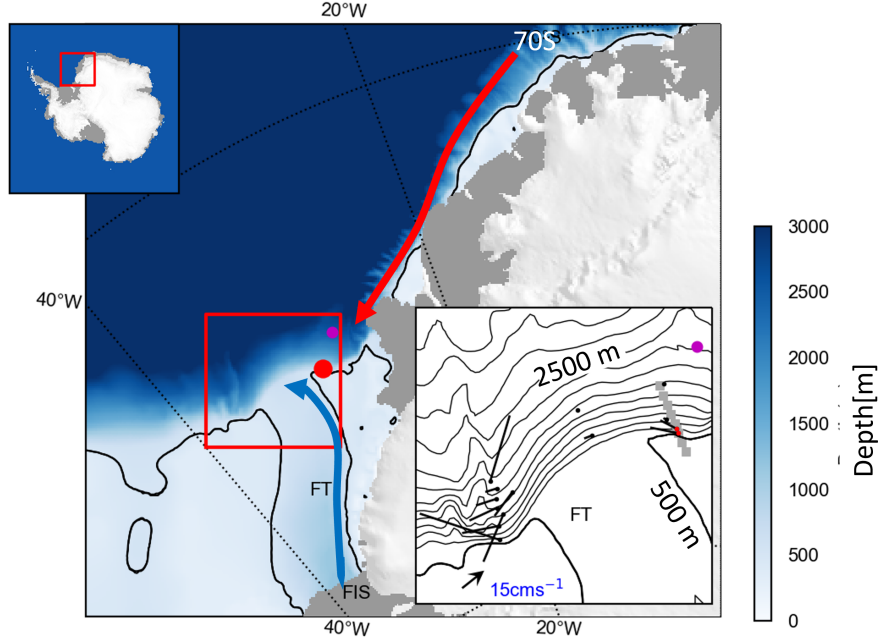


Figure 1. Map over the study area with bathymetry (Fretwell et al., 2013) in blue shading according to the colorbar. The 500 m isobath is highlighted in black. The circulation in the area is shown with blue (outflow of ISW) and red (slope front and coastal current) arrows (Darelius et al., 2014; Ryan et al., 2017), and the positions of the $M_{530/740}$ (red circle), M_{2570} (magenta triangle), Kapp Norvegia (black pentagon) moorings and moorings at 76°S (cyan squares) are indicated. Floating ice shelves are shown in dark gray and land in light gray. FT indicates the Filchner Trough, KN is Kapp Norvegia, and FIS is the Filchner Ice Shelf. The insets show (upper, left) the position of the study area and (lower, right) a zoom-in to the area marked with a red rectangle in the main figure, covering the upper part of the continental slope at the FT opening. In the latter, positions of the CTD-section shown in Fig. 2 are marked with green squares and mean currents (25 mab) from historical moorings (black dots, Foldvik et al., 2004; Jensen et al., 2013; K. B. Daae et al., 2017) and M_{740} and M_{530} (red dots) are shown as sticks. The blue arrow on the continental shelf in the lower left corner gives the velocity scale. Isobaths are shown every 250 m, with the 500 m isobath in bold.

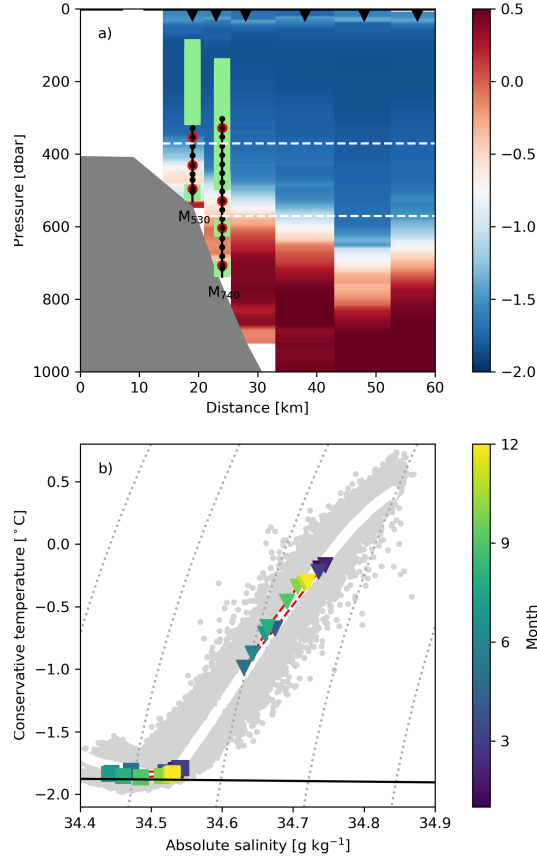


Figure 2. a) Temperature sections across the continental slope at the position of mooring M₇₄₀ and M₅₃₀ (roughly along 30°W, see Fig. 1 for location) occupied 25 February (duration 17 h) in 2017. The position of individual CTD profiles is indicated with black triangles at the upper y-axis. The position of the moorings is indicated in (a), where black dots denote temperature sensors, red circles salinity sensors, and where levels with velocity records are marked in green. The dashed white lines show the target depth of the temperature sensors at M₂₅₇₀. b) Θ - S_A diagram showing monthly mean hydrography from M₇₄₀ at 707 m (triangles) and 328 m (squares) depth color-coded with respect to time. The grey dots show the complete hydrography record from the mooring, while the CTD-cast occupied in the vicinity of the mooring site on recovery (February 2021) is shown in white.

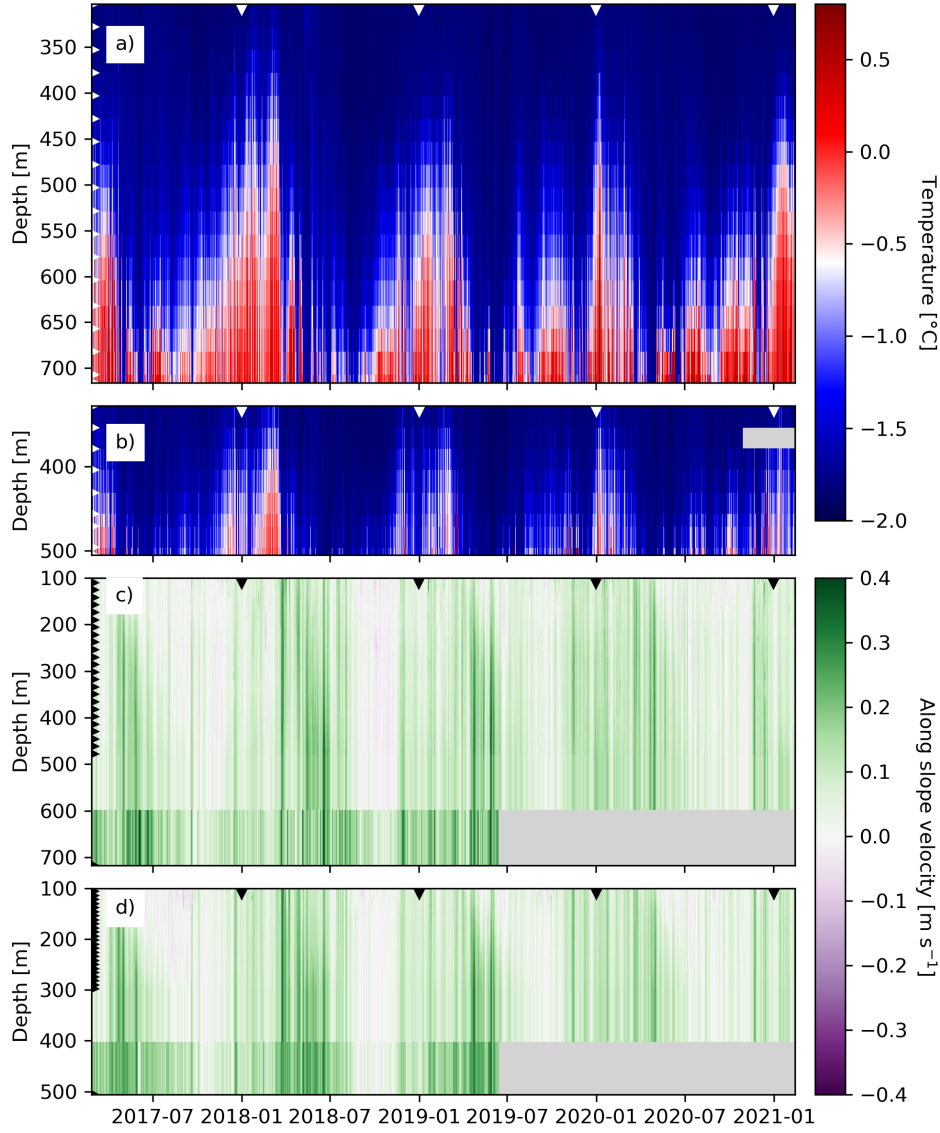


Figure 3. Hovmöller diagram of temperature at a) M_{740} and b) M_{530} . Hovmöller diagram of alongslope velocity at c) M_{740} and d) M_{530} . Triangles at the y-axis show the measurement depths, and the triangles on the upper x-axis mark 1 January of each year. The current meter data are low-pass filtered using a 5th-order Butterworth filter with a cut-off period of 48 h to remove tides and topographic Rossby waves (Jensen et al., 2013). Note that the vertical scale differs between (a-b) and (c-d) and that the lower ADCP bin and point measurement of velocity are extended vertically over >100m. Periods without data are marked in grey

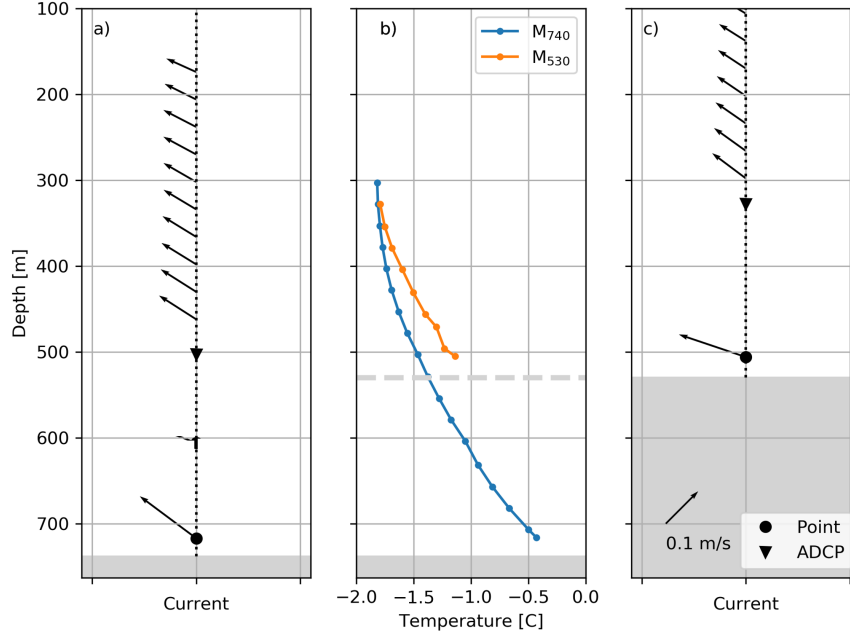


Figure 4. Time-averaged a) current profile from M₇₄₀, b) temperature profiles from M₇₄₀ and M₅₃₀ according to the legend and c) current profile for M₅₃₀. The bottom depth is indicated in grey, where the dashed grey line in (b) is the bottom depth at M₅₃₀ and the filled box the bottom depth at M₇₄₀. The scale arrow in the lower left corner of (c) is valid for (a) and (c), and the velocity vectors shown are horizontal velocities. For clarity, results from every other (every fourth) ADCP-bin are shown in a(c).

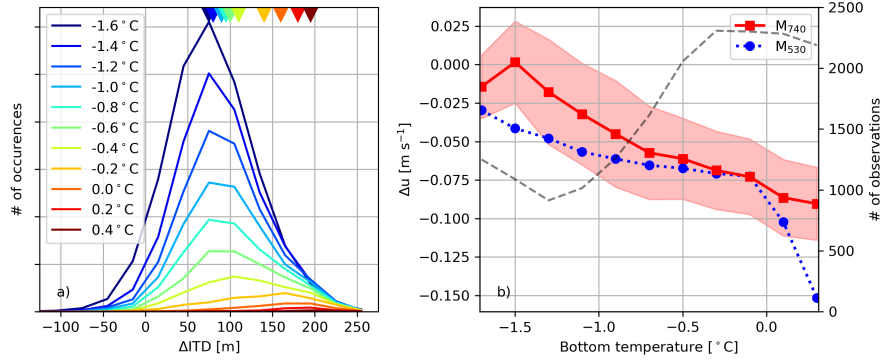


Figure 5. a) Line histograms of ΔITD for isotherms according to the legend. The colored triangles at the upper x -axis show the time-averaged value of ΔITD for the respective isotherm. Positive values indicate that the isotherm is higher up in the water column on M_{530} than on M_{740} . b) Time-averaged difference in along slope velocity (Δu) between the two lowest levels with current measurements (see Table 1) in $0.2^\circ C$ wide temperature bins for M_{740} (red squares) and M_{530} (blue circles). Negative values indicate that the velocity decreases upward. The shading shows a conservative estimate of the standard error (see sec. 2.1) for Δu (for M_{740}), and the dashed line shows the number of observations within each bottom temperature bin for M_{740} .

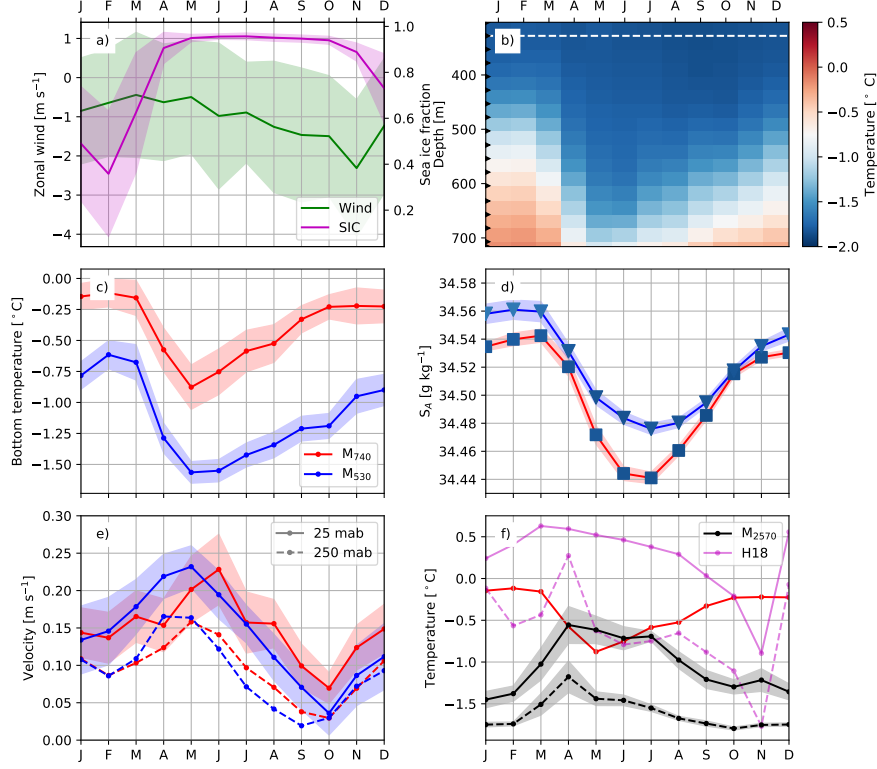


Figure 6. Mean seasonal cycle of a) local zonal wind and sea ice concentration, b) temperature as a function of depth at M_{740} , c) bottom temperature d) upper-level Absolute Salinity at M_{740} (328 m, squares / red line, dashed white line in panel b) and M_{530} (354 m, triangles / blue line), e) along-slope velocity, and f) temperature at mooring M_{2570} at 571 m (black line) and 371 m (dashed, black line) depth. The mean seasonal cycle in bottom temperature at M_{740} (red line, from panel c) and the seasonal cycle extracted from the Kapp Norvegia climatology (marked H18 in the legend, Hattermann, 2018) at similar isobath and depths are included for comparison (magenta lines). In (b), the black triangles on the y-axis show the depth of the sensors, and in (a, c-f), the shaded area shows the standard error. The color of the markers in panel (c) shows the temperature at the same depth using the color scale from panel (b).

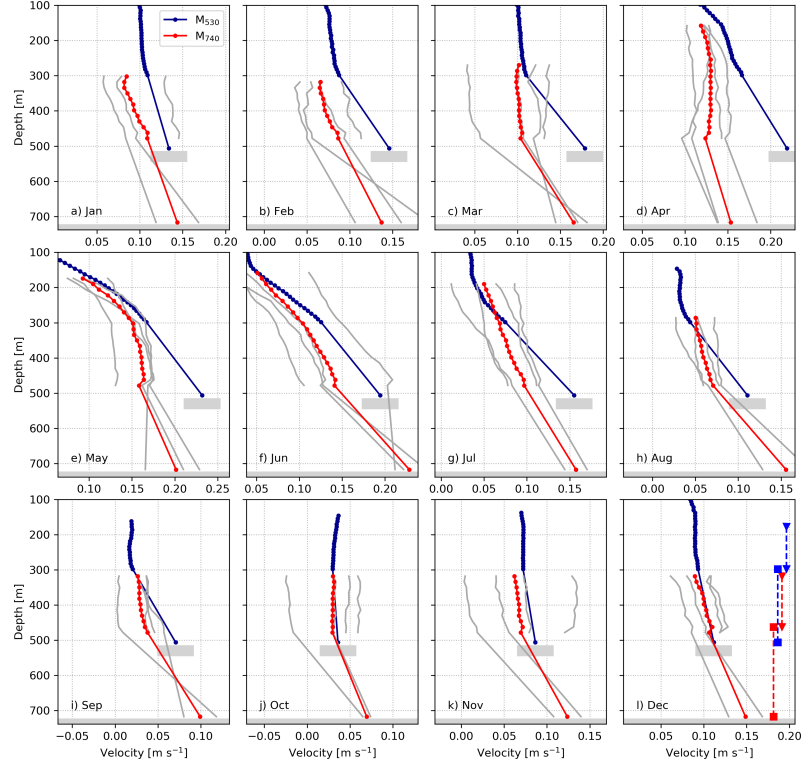


Figure 7. Deployment mean vertical profiles of along-slope velocity for a) January, b) February, c) March, d) April, e) May, f) June, g) July, h) August, i) September, j) October, k) November and l) December at M₇₄₀ (red) and M₅₃₀ (blue). Monthly mean profiles from individual years at M₇₄₀ are shown in grey. The velocity scale is centered around the value observed at M₇₄₀, 300 m depth, but the range shown is the same in all panels so that gradients are comparable. The dashed lines in (l) show the vertical range of Δu shown in Fig. 9.

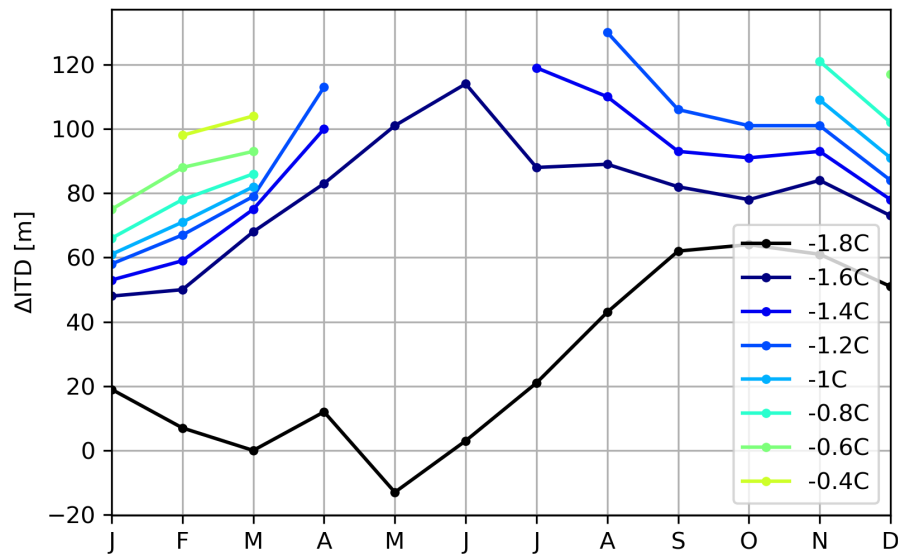


Figure 8. Monthly mean ΔITD for isotherms according to the legend. Only values for months when the isotherm was within the vertical range of the two moorings more than 25% of the time are shown.

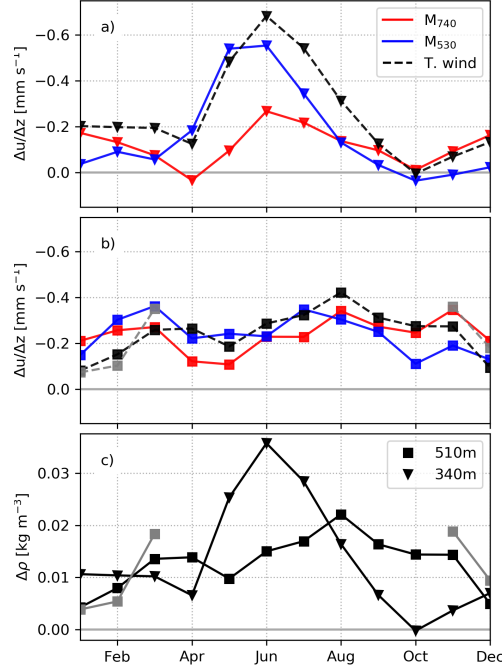


Figure 9. Monthly mean vertical gradients in along slope velocity over a) the middle and b) the lower part of the water column. The dashed lines show the vertical velocity gradient estimated from the horizontal density difference between the two moorings (thermal wind) with density calculated from the observed temperature and salinity (black) and temperature only using eq. 2 (grey). Only months for which the temperature is within the temperature range for which eq. 2 is valid ($-1.5 < \Theta < 0.4^\circ\text{C}$) at both moorings more than 75% of the time are shown. The depth ranges used for the different layers and moorings are indicated in Fig. 71. Note that the y-axis is reversed. Negative values indicate that the velocity increases towards the bottom. c) Monthly mean *in situ* density difference between M_{740} and M_{530} at about 510 m (squares) and 340 m (triangles) depth calculated from observed salinity and temperature (black) and temperature only (grey). Positive values indicate that the density at M_{530} is higher. Note that there is a $\simeq 30\text{m}$ difference in the depth of the sensors at the two moorings. The figure is based on data recorded before June 2019, when the lower current meters stopped recording.

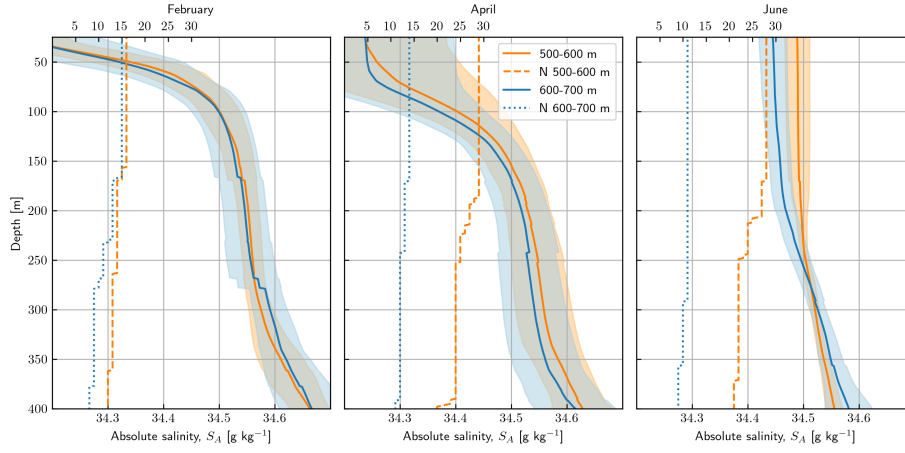


Figure 10. Monthly mean profiles of Absolute Salinity (continuous lines) collected by instrumented Weddell Seals between the 500-600 m isobath (orange) and the 600-700 m isobath (blue) in the shelf break region upstream of FT. The standard deviation is given by color shading, and the number of profiles included in the mean profiles is indicated by the dashed lines, following the upper horizontal axis. Only profiles with a thick (>150 m) WW layer ($\Theta < -1.8^\circ \text{C}$) are included.

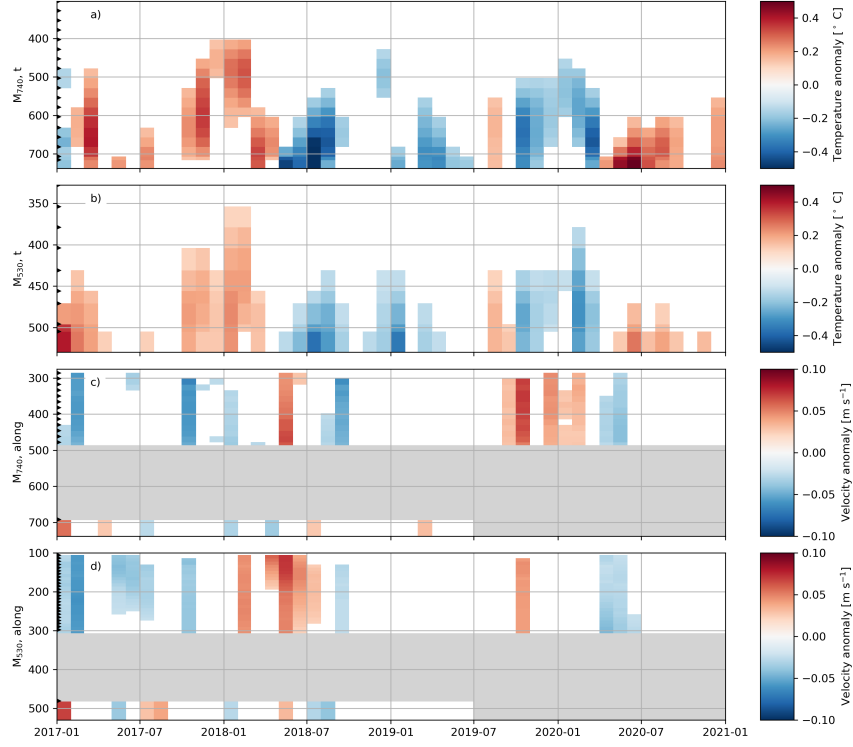


Figure 11. De-seasoned, monthly mean anomalies of temperature at a) M_{740} and b) M_{530} and of along slope velocity at c) M_{740} and d) M_{530} . For clarity, only levels and months where the anomaly is larger than one standard deviation are shown, and the depth ranges without velocity measurements are colored grey. Note that the current meters at 25 mab stopped recording in June 2019 on both moorings.

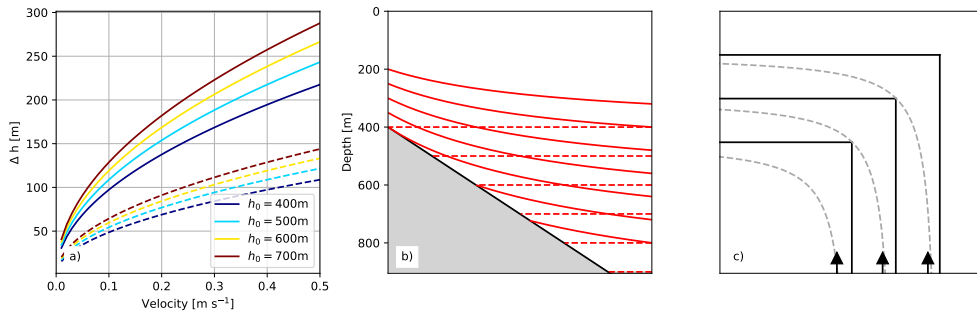


Figure 12. a) Change in depth (Δh) for the turning jet as a function of velocity, for different initial depth of the streamlines (h_0 , color according to legend) and slope ($\nabla h = 0.04$ solid lines and $\nabla h = 0.01$ dashed lines). b) Position of (initially horizontal) isotherms after a $\Delta h = 200\text{m}$ onshore shift. c) Sketch showing the streamlines (dashed lines) of a barotropic jet encountering a corner in the bathymetry (black lines) in the southern hemisphere. The current enters from the lower bottom (black arrows) and deeper water is to the right of the current (freely after Williams et al., 2001, , their Fig. 5).